Incorporating adaptive optics controls history in post-processing of ground-based coronagraph models

Leonid Pogorelyuk, Christian Delacroix, Gilles Orban de Xivry, Kerri Cahoy, N. Jeremy Kasdin

Leonid Pogorelyuk, Christian Delacroix, Gilles Orban de Xivry, Kerri L. Cahoy, N. Jeremy Kasdin, "Incorporating adaptive optics controls history in post-processing of ground-based coronagraph models," Proc. SPIE 11448, Adaptive Optics Systems VII, 1144854 (13 December 2020); doi: 10.1117/12.2562262

SPIE.

Event: SPIE Astronomical Telescopes + Instrumentation, 2020, Online Only

Incorporating Adaptive Optics Controls History in Post-processing of Ground-based Coronagraph Models

Leonid Pogorelyuk[a], Christian Delacroix[b], Gilles Orban de Xivry[b], Kerri L. Cahoy[a], and N. Jeremy Kasdin[c]

[a]Department of Aeronautics and Astronautics, Massachusetts Institute of Technology, 77 Massachusetts Avenue, Cambridge, MA 02139, USA
[b]Space Sciences, Technologies, and Astrophysics Research Institute, Université de Liège, B-4000 Sart Tilman, Belgium
[c]University of San Francisco, College of Arts and Sciences, 2130 Fulton St., San Francisco, CA, US, 94117

ABSTRACT

The planet detection thresholds of space-based coronagraphs are predicted to lie within an order of magnitude from their theoretical (shot-noise) limits. Ground-based telescopes, on the other hand, are limited by larger systematic uncertainties in the point spread function (PSF) of the residual light which rapidly fluctuates due to atmospheric turbulence. The PSF is affected by Adaptive Optics (AO) which reduce the intensity of the speckles but also make them less predictable. Although not a common practice, it is possible to take millisecond exposures of the so-called "frozen" speckles and record the history of AO controls, in which case the collected data resembles that of simulated space coronagraphs. In this work we use the HEEPS simulation of the E-ELT/METIS to assess the applicability of this newly-developed space-oriented approach to ground-based post-processing. Unlike intensity-based algorithms, this method formulates the estimation problem in terms of the electric field of the speckles and therefore can incorporate controls history and various temporal models of the electric field variations. In our simulations, we artificially introduced small deformable mirror (DM) probes on top of AO controls, and achieved a post-processing error lower by a factor of 2 than that of Angular Differential Imaging (ADI). However, our attempt at incorporating the AO history without DM probes, has so far resulted in higher errors than ADI.

Keywords: High-contrast imaging, Post-processing, Deformable Mirrors, ADI, Order Reduction, Electric Field

1. INTRODUCTION

The contrast between the signal of an exoplanet and its host star, viewed from a ground-based telescope, is limited by the ability of Adaptive Optics (AO) to reject wavefront perturbations caused by atmospheric turbulence.[1,2] Even when the speckles (post-AO residual starlight) are brighter than the planet, the planet signal may still be recovered by post-processing multiple consecutive exposures on the target star.[3,4]

Most of the existing post-processing methods explicitly or implicitly estimate the *intensities* of the speckles at every exposure, subtract them, and average the remaining signal. For example, Reference Differential Imaging (RDI) estimates speckle intensities based on previous observations. It includes approaches that construct a library of speckle patterns that can be projected out, such as Karhunen-Loéve Image Projection (KLIP)[5] and Non-negative Matrix Factorization (NMF).[6] The performance of such methods depends heavily on the size of the patterns library (i.e., number of intensity modes), which scales unfavorably with the dimensionality of the pre-coronagraph wavefront perturbation (e.g., the number of Zernike polynomials describing the wavefront error in the pupil plane).[7]

Further author information send correspondence to Leonid Pogorelyuk, E-mail: leonidp@mit.edu

Adaptive Optics Systems VII, edited by Laura Schreiber, Dirk Schmidt, Elise Vernet, Proc. of SPIE
Vol. 11448, 1144854 · © 2020 SPIE · CCC code: 0277-786X/20/$21 · doi: 10.1117/12.2562262

Other intensity-based approaches, exploit the difference in the physical behavior of speckles and sources incoherent with the starlight (e.g., planets). Angular Differential Imaging (ADI)[8] rotates the images such that the speckles, that are (at least partially) fixed to the telescope, self-subtract, while the incoherent sources that do not rotate with the telescope persist. Similarly, Spectral Differential Imaging (SDI)[9] exploits the scaling that speckles exhibit as a function of wavelength while the positions of the exoplanets (i.e, the maxima of their PSF) remain fixed.

Physical effects that help distinguish between speckles and planets can also be introduced artificially. Splitting and phase-shifting the starlight[10] or introducing apodizers,[11] can produce starlight interference patterns in the focal plane, from which the speckles can be estimated (for a review of focal-plane methods see Jovanovic *et al.* 2018[12]). Deformable mirrors (DM) are also used for focal-plane estimation of the *electric field* of the speckles in order to increase the contrast throughout both ground-based[13] and future space-based observations (i.e., Electric Field Conjugation (EFC)[14]).

In this work, we examine how small DM probes (on top of AO) may facilitate post-processing. Similarly to focal-plane wavefront control (e.g., EFC), post-processing which involves the DM has to be stated in terms of the electric-field, and similarly to ADI, it has to account for the rotation of the planet signal between different exposures. The authors have recently extended Electric Field Order Reduction (EFOR)[15] to account for the DM and for telescope rotations in the context of space-based telescopes. Unlike COFFEE (COrona-graphic Focal-plane wave-Front Estimation for Exoplanet detection),[16] EFOR doesn't propagate an optical model of the instrument but rather estimates a small basis for the electric field of the speckles based on observations alone.

In the rest of this section we provide a brief overview of EFOR. In Section 2 we describe our simulation of the METIS (Mid-infrared E-ELT Imager and Spectrograph) instrument of the E-ELT (European Extremely Large Telescope),[17] and compare ADI and EFOR post-processing approaches. In particular, our simulations show that under some favorable assumptions, the introduction of small known electric field perturbations (via DM probes), may decrease the post-processing by a factor of 2 compared to ADI.

1.1 Electric Field Order Reduction (EFOR)

EFOR is a numerical procedure which estimates the intensity of sources incoherent with the starlight (e.g. planets). This intensity is denoted as $\mathbf{I}^P \in \mathbb{R}^N$ where N is the number of pixels in the high-contrast region of interest (the dark hole). Besides measurements from K exposures, $\{\mathbf{y}(k)\}_{k=1}^K \subset \mathbb{N}^N$, EFOR also requires applying small probes with the deformable mirrors throughout the observations. Although the fast-varying electric field at the image plane is not known, the major underlying assumption is that the *contributions* of the probes to the electric field in the image plane, $\left\{\delta\mathbf{E}^{DM}(k)\right\} \subset \mathbb{R}^{2cN}$, are known (the complex electric field is treated as a vector of real numbers and c is the number of wavelengths in the discretization of the model). We note that the probes need not be very precisely known, since their zero-mean uncertainties are implicitly estimated by EFOR.

We begin with the definition of the intensity vectors of all sources, $\mathbf{I}(k) \in \mathbb{R}^N$. The contributing sources are split into speckles, signal (e.g., planets), and other sources (e.g., thermal background),

$$\mathbf{I}(k) = \underbrace{B \cdot \mathbf{E}^{\circ 2}(k)}_{\text{speckles}} + \underbrace{R(k)\mathbf{I}^P}_{\text{signal}} + \underbrace{\mathbf{I}^D}_{\text{other sources}}, \tag{1}$$

where $\mathbf{E}(k) \in \mathbb{R}^{2cN}$ is the electric field of the speckles discretized into c spectral channels, B is a linear operation of summation over all the components of each pixel ($B = I_{N\times N} \otimes \mathbf{1}_{2c}$, $I_{N\times N}$ is the identity matrix, $\otimes$ denotes the Kronecker product and $\mathbf{1}_{2c} \in \mathbb{R}^{1\times 2c}$ the vector of ones), $\mathbf{I}^P \in \mathbb{R}^N$ is the intensity of planets, zodi, etc., $R(k) \in \mathbb{R}^{N\times N}$ is a rotation matrix that transforms the signal $\mathbf{I}^P$ based on the orientation of the telescope at exposure k, and $\mathbf{I}^D \in \mathbb{R}^N$ is the intensity of other sources incoherent with the starlight that are assumed to be known (e.g., thermal background).

The measurements, $\mathbf{y}(k) \in \mathbb{R}^N$, depend on the intensity but are non-deterministic. In general, the probability of measuring $\mathbf{y}(k)$ given $\mathbf{I}(k)$ is $p\left(\mathbf{y}(k)\middle|\,\mathbf{I}(k)\right)$. In the numerical simulations we assumed each ith element of $\mathbf{y}$ corresponds to photon counts and is Poisson distributed with expectation equal to the ith element of $\mathbf{I}\Delta t$,

$$p\left(y_i(k)\middle|\,I_i(k)\right) = \frac{(I_i(k)\Delta t)^{y_i(k)}\, e^{-I_i(k)\Delta t}}{y_i(k)!}, \tag{2}$$

where Δt is the exposure time. Under this assumption, and if the electric fields $\{\mathbf{E}(k)\}_{k=1}^{K}$ were known, Eq. (1) could be averaged to show the dependence of the signal on the measurements

$$\mathbf{I}^P \approx \frac{1}{K}\sum_{k=1}^{K} R^{-1}(k)\left(\frac{1}{\Delta t}\mathbf{y}(k) - B\cdot\mathbf{E}^{\circ 2}(k) - \mathbf{I}^D\right), \tag{3}$$

where K is the number of exposures.

However, the number of measurements, $N\cdot K$, is smaller than the number of unknown electric field elements $2cN\cdot K$ resulting in an underdetermined estimation problem. We make the problem overdetermined by assuming that the electric fields lie in an r dimensional subspace spanned by the columns of an *a-priori* unknown matrix $G^V \in \mathbb{R}^{2cN\times r}$,[7] i.e.,

$$\mathbf{E}(k) = G^V\mathbf{v}(k) + \delta\mathbf{E}^{DM}(k),\ 1\le k\le K \tag{4}$$

where $\{\mathbf{v}(k)\}_{k=1}^{K}\subset\mathbb{R}^r$ are *a-priori* unknown vectors of mode coefficients and $\left\{\delta\mathbf{E}^{DM}(k)\right\}_{k=1}^{K}\subset\mathbb{R}^{2cN}$ are known DM contributions to the electric fields at each exposure. With $r\ll N,K$, this order reduction technique leaves us with a relatively small number of unknowns, $2cN\cdot r + r\cdot K \ll N\cdot K$.

Denoting the estimates of the modes and their coefficients as $\hat{G}$ and $\{\hat{\mathbf{v}}(k)\}_{k=1}^{K}$ respectively, estimates of the electric field are

$$\hat{\mathbf{E}}(k) = \hat{G}\hat{\mathbf{v}}(k) + \delta\mathbf{E}^{DM}(k),\ 1\le k\le K. \tag{5}$$

We now slightly modify Eq. (3) to get an estimate of the signal as a function of $\hat{G}$ and $\{\hat{\mathbf{v}}(k)\}_{k=1}^{K}$,

$$\hat{\mathbf{I}}^P\left(\hat{G}^V, \{\hat{\mathbf{v}}(k)\}_{k=1}^{K}\right) = \mathcal{R}\left\{\frac{1}{K}\sum_{k=1}^{K} R^{-1}(k)\left(\frac{1}{\Delta t}\mathbf{y}(k) - B\cdot\left(\hat{G}\hat{\mathbf{v}}(k) + \delta\mathbf{E}^{DM}(k)\right)^{\circ 2} - \mathbf{I}^D\right)\right\}, \tag{6}$$

where $\mathcal{R}$ is the elementwise ramp function (which prevents numerical issues caused by negative intensity estimates).

The parameters $\hat{G}$ and $\{\hat{\mathbf{v}}(k)\}_{k=1}^{K}$ are found numerically by maximizing the log-likelihood of the measurements,

$$L = \sum_{k=1}^{K}\log p\left(\mathbf{y}(k)|\, B\cdot\left(\hat{G}^V\hat{\mathbf{v}}(k) + \delta\mathbf{E}^{DM}\right)^{\circ 2} + R(k)\hat{\mathbf{I}}^P + \mathbf{I}^D\right), \tag{7}$$

with p given elementwise in Eq. (2). Note that this is a simultaneous optimization over all the parameters since each element in the above summation depends on all $\hat{\mathbf{v}}(k)$ through $\hat{\mathbf{I}}^P$. Specifically, $\hat{G}^V$ is initialized as a matrix of orthonormal columns, $\hat{\mathbf{v}}(k)$ are initialized as zeros for all k, and $-L$ is minimized via gradient descent.

2. NUMERICAL COMPARISON OF ADI AND EFOR WITH HEEPS AND COMPASS

In this section we compare the performance of ADI and EFOR on data generated by High-contrast End-to-End Performance Simulator (HEEPS) of METIS[18,19] from AO residuals generated by COMputing Platform for Adaptive optics SystemS (COMPASS).[20] The details of the simulation are described in Sec. 2.1, and in Sec. 2.2 we show that EFOR may outperform ADI under some favorable assumptions. First, EFOR relies on photon counting detectors that operate on the same millisecond time scales as the DM.[21] Second, it requires introducing DM probing (small actuations on top of AO) throughout the observation and knowing their electric-field contribution as discussed in Sec. 2.4. One could potentially incorporate the full history of the AO controls instead of probing the DM, however we failed to reach a higher accuracy that way (Sec. 2.3).

2.1 System Description

The phase aberrations at the pupil plane, partially corrected by AO, were first simulated by COMPASS at 1 ms cadence and then propagated with HEEPS. To save computation time, we only simulated and propagated $K = 400$ AO residual phases for the first 400 ms of every minute, for 60 minutes.

The light from a 6 magnitude star was simulated at a single wavelength of 3.8 μm, collected with a 37 m pupil with 30% central obscuration and passing through a classical vortex coronagraph. In our simulation, the 5.2 mas wide pixels received on average $0.04 - 0.9$ photons per second (at 15 and 5 λ/D respectively). Planet signals of magnitude 17 were added in a grid pattern as illustrated in Fig. 1(b) which was then rotated to match the orientation of the telescope at every minute. The photon counts were sampled form a Poisson distribution every $\Delta t = 1$ ms, after the speckle electric fields were augmented with DM probes (see Sec. 2.4).

Even with most of the data discarded (59.6 seconds out of every minute), the EFOR optimization described in Sec. 1.1 required 36 GB of memory and ran for tens of minutes on a GPU.

2.2 Results

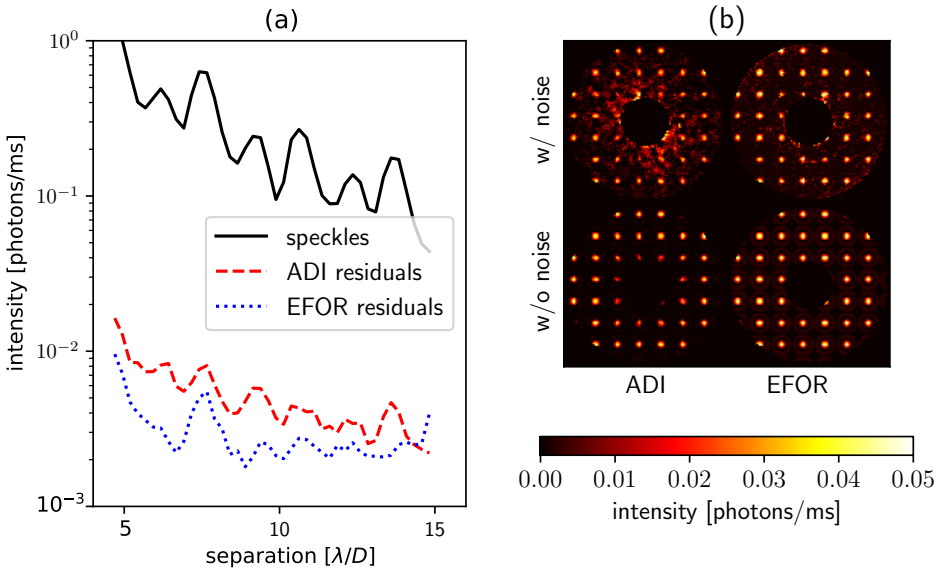

Figure 1. (a) The average intensity of the speckles (solid black line) compared to the standard deviation of the post-processing errors of ADI (dashed red line) and EFOR (dotted blue line). In our example, ADI increases the effective contrast by two orders of magnitude by exploiting field rotations. EFOR also utilizes DM probes to estimate the temporal variations in the electric field of the speckles. Given photon-counting measurements at 1 ms resolution and known DM probes (see Sec. 2.3 and 2.4), EFOR improves upon ADI by a factor of about 2. (b) Comparison between images post-processed by ADI (left) and EFOR (right) with (top) and without (bottom) noise due to speckles and finite exposure time. Fake planets were injected on a grid and were well-recovered by both methods at high angular separations (towards the outer edge of the dark hole ring). At lower separations, EFOR is better at estimating and subtracting the speckles (note the self-subtraction typical of ADI, bottom left).

Figure 1(b) shows the post-processed results when using ADI and EFOR. The image at the bottom of Fig. 1(b) represents the results expected from both approaches in the absence of speckles or shot-noise. At small angular separations ($< 10\lambda/D$), ADI suffers from both brighter speckles and self-subtraction[22] (the peaks of the expected PSF are lower than that of the signal PSF), while EFOR estimates the incoherent signal directly.

Figure 1(a) shows the averaged difference between expected and post-processed signals as a function of angular separation. ADI alone increases the signal-to-noise ratio (S/N) by two orders of magnitude and EFOR improves upon ADI by another factor of about two. The improvement is most noticeable at low angular separations due to

the aforementioned self-subtraction. We note that these results were achieved under the favorable assumptions of measuring photon counts at 1 ms resolution and adding small known DM contribution to the electric field.

2.3 Failure to Incorporate Full AO Telemetry without DM Probes

Although not a common practice during ground-based observation, one could store the history of the voltages that the AO controller applied during an observation. Instead, in our simulations, we had access to both the closed-loop (post-AO) electric fields, $\mathbf{E}(k)$, and the hypothetical open-loop fields, $\mathbf{E}^{OL}(k)$, that would occur in the absence of AO. We therefore treated their difference, $\mathbf{E}^{DM}(k) = \mathbf{E}(k) - \mathbf{E}^{OL}(k)$, as the known history of DM "contributions" and assessed its usability in post-processing. Note that the full AO contribution, $\mathbf{E}^{DM}$, is much larger than the probes used in EFOR, $\delta\mathbf{E}^{DM}$ and that ideally, the knowledge of $\mathbf{E}^{DM}(k)$ would render probing unnecessary.

For most pixels, $1 \leq i \leq N$, we have found the increments of the DM contribution, $E_i^{DM}(k+1) - E_i^{DM}(k)$, to be correlated with the increments of the closed loop-electric field, $E_i(k+1) - E_i(k)$. This temporal dependency could be incorporated into the post-processing procedure described in Sec. 1.1 by adding the following penalty to the cost function defined in Eq. (7),

$$L^{DM} = \alpha \sum_{i,k} \left(\left(E_i^{DM}(k+1) - E_i^{DM}(k) \right)^2 - \left(E_i(k+1) - E_i(k) \right)^2 \right),$$

where α is a free parameter (which depends on how strong the correlation between $E_i^{DM}(k+1) - E_i^{DM}(k)$ and $E_i(k+1) - E_i(k)$ is).

Unfortunately, this approach led to post-processing errors that were significantly higher than ADI and EFOR (with artificial probes). We suspect that the above penalty, L^{DM}, may not capture the connection between DM contributions and the closed-loop electric field with the $\sim 1\%$ accuracy required to distinguish between speckles and signal (since ADI alone, increases the S/N by a factor of about 100, see Fig. 1(a)). Moreover, since $\mathbf{E}^{DM}$ will not be known during observations, we did not pursue this direction further. We leave the search for a more sophisticated penalty function that incorporates the optical model of the instrument (similarly to COFFEE[16]) for future work.

2.4 Approximating DM Probes and their Effects

Since the AO residual phases provided by COMPASS did not include DM probes, they had to be artificially added. This was done by randomly selecting small electric fields, $\delta\mathbf{E}^{DM}$, to be added to the post-AO electric field simulated by HEEPS. The added electric field was chosen in a subspace empirically estimated as follows: the known closed-loop and open-loop electric fields, $\mathbf{E}(k)$ and $\mathbf{E}^{OL}(k)$ respectively, were subtracted and the resulting time differences were arranged into a matrix,

$$\Phi = \begin{bmatrix} \cdots & \mathbf{E}^{DM}(k+1) - \mathbf{E}^{DM}(k) & \cdots \end{bmatrix} \in \mathbb{R}^{2N \times K}.$$

The DM probes were then chosen as a random linear combination of the columns of Φ, i.e, $\delta\mathbf{E}^{DM}(k) \in \text{colspace}\Phi$.

In practice, the probes would have to be introduced by small but known DM commands, $\delta\mathbf{u}(k)$. These commands would then need to be translated into their effect on the electric field $\delta\mathbf{E}^{DM}(k)$. This "translation" will be dependent on the telescope's model and calibration, and the systematic errors involved will affect the post-processing results (although they will be partially mitigated by EFOR). In the context of a space-based coronagraph, DM voltages are translated into electric-field contributions with the help of the sensitivity matrix (Jacobian) which is estimated based on the optical model.[23] Although, imperfect knowledge of the Jacobian translates into uncertainties in the probes, $\delta\mathbf{E}^{DM}$, these errors are zero-mean (when the probes are), and are implicitly estimated by EFOR (see Eq. (5)). We leave the quantitative analysis for future work.

The post-processing error depends on the magnitude of the probes (e.g., the average $\left\|\delta\mathbf{E}^{DM}\right\|$). Larger probes introduce more phase diversity and increase the accuracy of the electric field estimates, thus facilitating their subtraction. However, they also introduce more starlight into the image plane, resulting in higher shot-noise. This tradeoff is illustrated in Figure 2 by looking at the dependency of post-processing error on the number

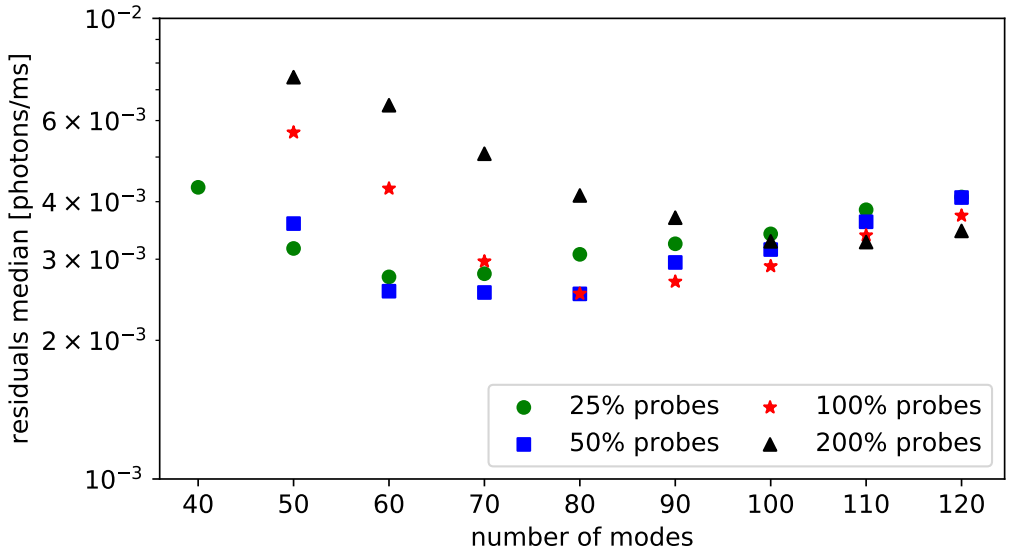

Figure 2. Median residual errors of EFOR as a function of probe magnitude and the number of modes used for fitting the electric field (the median is across all separations in Fig. 1(a)). For a fixed probe magnitude, a small number of electric field modes modes is insufficient to fit the data, while too many modes overfit it. As the probe magnitude increases, the "optimal" number of modes increases (the observations contain more information which, reduces overfitting). Although probes above the "optimal" magnitude (denoted by red stars) allow for a better fitting of the electric field, they also introduce significantly more light into the dark hole, resulting in larger post-processing error due to shot noise.

of estimated electric field modes, r. For any fixed probe magnitude, there exists an optimal r below which the speckles are not well represented by a small number of modes and above which the data is overfitted by too many degrees of freedom. The stronger the probes, the larger the number of modes that can be accurately estimated before overfitting occurs is, but the images are also noisier. The results for Fig. 1 correspond to the choice of r and average $\left\|\delta\mathbf{E}^{DM}\right\|$ that lead to highest post-processing S/N.

3. CONCLUSIONS

In this work we demonstrated that formulating the post-processing problem in terms of the image-plane electric field (rather than intensity) can potentially increase the S/N by a factor of about 2. However, since the electric field is not measured directly, our approach requires the introduction of phase diversity via the DM. In our simulations, we were unable to utilize AO telemetry (the history of DM voltages) for this purpose. Instead, we introduced small DM probes on top of the DM commands (AO correction), and assumed that their contribution to the electric field of the speckles is known. Although this assumption is typical in space-based coronagraphy in the context of EFC, it is now being considered for ground-based telescopes as well.[24,25]

In principle, wavefront sensing (WFS) telemetry should provide some information that acts as a statistical prior and enhances the post-processing results, if properly incorporated in EFOR's cost function. In Sec. 2.3 we tried, without success, penalizing the difference between the uncorrected and AO-corrected electric field increments (as they seem to be correlated). We suspect that the systematic errors in our simplistic first-order correlation model are larger than ADI residuals, leading to a worse S/N. We leave the model-based statistical analysis necessary to incorporate WFS telemetry without DM probes in EFOR's cost function for future work.

Another favorable assumption that we made in our analysis was the availability of high-frequency photon counting measurements. Such devices, being currently under development,[21] will be necessary to "resolve" the fast changes in the speckle's electric field. We note that even though the photon arrival rate from the target star will probably be insufficient to estimate the electric field of the speckles at each exposure, over the course of millions of exposures, we expect EFOR to accurately estimate the first few principal components of those fields.

4. ACKNOWLEDGEMENTS

The authors acknowledge the MIT SuperCloud and Lincoln Laboratory Supercomputing Center for providing High Performance Computing (HPC) resources that have contributed to the research results reported within this paper/report.

REFERENCES

[1] Guyon, O., "Limits of adaptive optics for high-contrast imaging," *The Astrophysical Journal* **629**(1), 592–614 (2005).

[2] Cavarroc, C., Boccaletti, A., Baudoz, P., Fusco, T., and Rouan, D., "Fundamental limitations on earth-like planet detection with extremely large telescopes," *Astronomy & Astrophysics* **447**(1), 397–403 (2006).

[3] Perrin, M. D., Maire, J., Ingraham, P., Savransky, D., Millar-Blanchaer, M., Wolff, S. G., Ruffio, J.-B., Wang, J. J., Draper, Z. H., Sadakuni, N., Marois, C., Rajan, A., Fitzgerald, M. P., Macintosh, B., Graham, J. R., Doyon, R., Larkin, J. E., Chilcote, J. K., Goodsell, S. J., Palmer, D. W., Labrie, K., Beaulieu, M., Rosa, R. J. D., Greenbaum, A. Z., Hartung, M., Hibon, P., Konopacky, Q., Lafreniere, D., Lavigne, J.-F., Marchis, F., Patience, J., Pueyo, L., Rantakyro, F. T., Soummer, R., Sivaramakrishnan, A., Thomas, S., Ward-Duong, K., and Wiktorowicz, S., "Gemini Planet Imager observational calibrations I: Overview of the GPI data reduction pipeline," in [*Ground-based and Airborne Instrumentation for Astronomy V*], *Proc.SPIE* **9147**, 1168 – 1180, International Society for Optics and Photonics, SPIE (2014).

[4] Gonzalez, C. A. G., Wertz, O., Absil, O., Christiaens, V., Defrère, D., Mawet, D., Milli, J., Absil, P.-A., Droogenbroeck, M. V., Cantalloube, F., Hinz, P. M., Skemer, A. J., Karlsson, M., and Surdej, J., "VIP: Vortex image processing package for high-contrast direct imaging," *The Astronomical Journal* **154**, 7 (jun 2017).

[5] Soummer, R., Pueyo, L., and Larkin, J., "Detection and characterization of exoplanets and disks using projections on Karhunen-Loève eigenimages," *The Astrophysical Journal Letters* **755**, L28 (aug 2012).

[6] Ren, B., Pueyo, L., Zhu, G. B., Debes, J., and Duchêne, G., "Non-negative matrix factorization: Robust extraction of extended structures," *The Astrophysical Journal* **852**, 104 (jan 2018).

[7] Pogorelyuk, L., Kasdin, N. J., and Rowley, C. W., "Reduced order estimation of the speckle electric field history for space-based coronagraphs," *The Astrophysical Journal* **881**, 126 (aug 2019).

[8] Marois, C., Lafreniere, D., Doyon, R., Macintosh, B., and Nadeau, D., "Angular differential imaging: A powerful high-contrast imaging technique," *The Astrophysical Journal* **641**(1), 556–564 (2006).

[9] Marois, C., Doyon, R., Racine, R., and Nadeau, D., "Efficient speckle noise attenuation in faint companion imaging," *Publications of the Astronomical Society of the Pacific* **112**, 91–96 (jan 2000).

[10] Bottom, M., Wallace, J. K., Bartos, R. D., Shelton, J. C., and Serabyn, E., "Speckle suppression and companion detection using coherent differential imaging," *Monthly Notices of the Royal Astronomical Society* **464**, 2937–2951 (10 2016).

[11] Codona, J. L., Kenworthy, M. A., Hinz, P. M., Angel, J. R. P., and Woolf, N. J., "A high-contrast coronagraph for the MMT using phase apodization: design and observations at 5 microns and 2 lambda/d radius," in [*Ground-based and Airborne Instrumentation for Astronomy*], *Proc.SPIE* **6269** (2006).

[12] Jovanovic, N., Absil, O., Baudoz, P., Beaulieu, M., Bottom, M., Cady, E., Carlomagno, B., Carlotti, A., Doelman, D., Fogarty, K., Galicher, R., Guyon, O., Haffert, S., Huby, E., Jewell, J., Keller, C., A.Kenworthy, M., Knight, J., Kühn, J., Miller, K., Mazoyer, J., N'Diaye, M., Por, E., Pueyo, L., Riggs, A. J. E., Ruane, G., Sirbu, D., Snik, F., Wallace, J. K., Wilby, M., and Ygouf, M., "Review of high-contrast imaging systems for current and future ground-based and space-based telescopes: Part II. common path wavefront sensing/control and coherent differential imaging," in [*Adaptive Optics Systems VI*], *Proc.SPIE* **10703** (2018).

[13] Codona, J. L. and Kenworthy, M., "Focal plane wavefront sensing using residual adaptive optics speckles," *The Astrophysical Journal* **767**, 100 (apr 2013).

[14] Give'on, A., Kern, B. D., Shaklan, S., Moody, D. C., and Pueyo, L., "Electric field conjugation-a broadband wavefront correction algorithm for high-contrast imaging systems," in [*Bulletin of the American Astronomical Society*], **39**, 975 (2007).

[15] Pogorelyuk, L., Pueyo, L., and Kasdin, N. J., "On the effects of pointing jitter, actuator drift, telescope rolls, and broadband detectors in dark hole maintenance and electric field order reduction," *Journal of Astronomical Telescopes, Instruments, and Systems* **6**(3), 1 – 14 (2020).

[16] Sauvage, J.-F., Mugnier, L., Paul, B., and Villecroze, R., "Coronagraphic phase diversity: a simple focal plane sensor for high-contrast imaging," *Opt. Lett.* **37**, 4808–4810 (Dec 2012).

[17] Quanz, S. P., Crossfield, I., Meyer, M. R., Schmalzl, E., and Held, J., "Direct detection of exoplanets in the 3–10 um range with e-elt/metis," *International Journal of Astrobiology* **14**(2), 279–289 (2015).

[18] Carlomagno, B., Absil, O., Kenworthy, M., Ruane, G., Keller, C. U., Otten, G., Feldt, M., Hippler, S., Huby, E., Mawet, D., Delacroix, C., Surdej, J., Habraken, S., Forsberg, P., Karlsson, M., Catalan, E. V., and Brandl, B. R., "End-to-end simulations of the E-ELT/METIS coronagraphs," in [*Adaptive Optics Systems V*], Marchetti, E., Close, L. M., and Véran, J.-P., eds., *Proc.SPIE* **9909**, 2070 – 2079, International Society for Optics and Photonics, SPIE (2016).

[19] Carlomagno, B., Delacroix, C., Absil, O., Cantalloube, F., Orban de Xivry, G., Pathak, P., Agocs, T., Bertram, T., Brandl, B. R., Burtscher, L., Doelman, D. S., Feldt, M., Glauser, A. M., Hippler, S., Kenworthy, M. A., Por, E. H., Snik, F., Stuik, R., and van Boekel, R., "METIS high-contrast imaging: design and expected performance," *Journal of Astronomical Telescopes, Instruments, and Systems* **6**(3), 1 – 30 (2020).

[20] Gratadour, D., Puech, M., Vérinaud, C., Kestener, P., Gray, M., Petit, C., Brulé, J., Clénet, Y., Ferreira, F., Gendron, E., Lainé, M., Sevin, A., Rousset, G., Hammer, F., Jégouzo, I., Paillous, M., Taburet, S., Yang, Y., Beuzit, J.-L., Carlotti, A., Westphal, M., Epinat, B., Ferrari, M., Gautrais, T., Lambert, J. C., Neichel, B., and Rodionov, S., "COMPASS: an efficient, scalable and versatile numerical platform for the development of ELT AO systems," in [*Adaptive Optics Systems IV*], Marchetti, E., Close, L. M., and Véran, J.-P., eds., *Proc.SPIE* **9148**, 2173 – 2180, International Society for Optics and Photonics, SPIE (2014).

[21] Meeker, S. R., Mazin, B. A., Walter, A. B., Strader, P., Fruitwala, N., Bockstiegel, C., Szypryt, P., Ulbricht, G., Coiffard, G., Bumble, B., Cancelo, G., Zmuda, T., Treptow, K., Wilcer, N., Collura, G., Dodkins, R., Lipartito, I., Zobrist, N., Bottom, M., Shelton, J. C., Mawet, D., van Eyken, J. C., Vasisht, G., and Serabyn, E., "DARKNESS: A microwave kinetic inductance detector integral field spectrograph for high-contrast astronomy," *Publications of the Astronomical Society of the Pacific* **130**, 065001 (June 2018).

[22] Mawet, D., Milli, J., Wahhaj, Z., Pelat, D., Absil, O., Delacroix, C., Boccaletti, A., Kasper, M., Kenworthy, M., Marois, C., Mennesson, B., and Pueyo, L., "Fundamental limitations of high contrast imaging set by small sample statistics," *The Astrophysical Journal* **792**, 97 (aug 2014).

[23] Marx, D., Seo, B.-J., Kern, B., Sidick, E., Nemati, B., and Poberezhskiy, I., "Electric field conjugation in the presence of model uncertainty," in [*Techniques and Instrumentation for Detection of Exoplanets VIII*], Shaklan, S., ed., *Proc.SPIE* **10400**, 188 – 196, International Society for Optics and Photonics, SPIE (2017).

[24] Por, E. H. and Keller, C. U., "Focal-plane electric field sensing with pupil-plane holograms," in [*Adaptive Optics Systems V*], Marchetti, E., Close, L. M., and Véran, J.-P., eds., *Proc.SPIE* **9909**, 1557 – 1573, International Society for Optics and Photonics, SPIE (2016).

[25] Matthews, C. T., Crepp, J. R., Vasisht, G., and Cady, E., "Electric field conjugation for ground-based high-contrast imaging: robustness study and tests with the Project 1640 coronagraph," *Journal of Astronomical Telescopes, Instruments, and Systems* **3**(4), 1 – 12 (2017).